

WaveGNN: Modeling Irregular Multivariate Time Series for Accurate Predictions

Arash Hajisafi*, Maria Despoina Siampou*, Bitu Azarijoo*, Cyrus Shahabi

Dept. of Computer Science, University of Southern California, Los Angeles, USA
 {hajisafi, siampou, azarijoo, shahabi}@usc.edu

Abstract

Accurately modeling and analyzing time series data is crucial for downstream applications across various fields, including healthcare, finance, astronomy, and epidemiology. However, real-world time series often exhibit irregularities such as misaligned timestamps, missing entries, and variable sampling rates, complicating their analysis. Existing approaches often rely on imputation, which can introduce biases. A few approaches that directly model irregularity tend to focus exclusively on either capturing intra-series patterns or inter-series relationships, missing the benefits of integrating both. To this end, we present **WaveGNN**, a novel framework designed to directly (i.e., no imputation) embed irregularly sampled multivariate time series data for accurate predictions. WaveGNN utilizes a Transformer-based encoder to capture intra-series patterns by directly encoding the temporal dynamics of each time series. To capture inter-series relationships, WaveGNN uses a dynamic graph neural network model, where each node represents a sensor, and the edges capture the long- and short-term relationships between them. Our experimental results on real-world healthcare datasets demonstrate that WaveGNN consistently outperforms existing state-of-the-art methods, with an average relative improvement of 14.7% in F1-score when compared to the second-best baseline in cases with extreme sparsity. Our ablation studies reveal that both intra-series and inter-series modeling significantly contribute to this notable improvement.

1 Introduction

The widespread use of sensors across various sectors, including healthcare, finance, astronomy, and urban applications [1–18], has led to a significant increase in the collection of time series data, ranging from univariate to multivariate types, where multiple measures are recorded simultaneously. Effectively modeling and analyzing these time series datasets is crucial for downstream applications such as monitoring patient health, optimizing treatments, and managing disease outbreaks, where accurate and timely data interpretation can significantly impact outcomes. In real-world applications, though, time series often exhibit irregularities, frequently caused by sensor malfunctions, different sampling rates across sensors, and cost-saving measures [19]. This variability in data collection renders traditional machine learning

(ML) approaches, which typically rely on a fixed number of regularly sampled observations across all sensors, ineffective for accurate predictions [19, 20].

Modeling irregularly sampled time series can be complex due to several factors: measurements from different sensors may not align, data may be missing, and each measurement sequence may vary in size [19, 21, 22]. To address these challenges, recent developments have concentrated on creating specialized algorithms and model architectures designed to effectively manage these irregularities [23].

One category of approaches tackles irregularity by filling in the missing values, thereby converting the datasets into regularly sampled time series. These imputation techniques vary from traditional hand-crafted imputation methods [24] to more advanced learned interpolation methods [21, 25]. Once the missing values are filled, the resulting regular time series are utilized to perform the downstream predictions [26–28]. While these techniques address data gaps, they introduce biases and distortions in the data distribution. Furthermore, the absence of measurements can itself provide valuable insights; for instance, periodically missing heart rate data might indicate that a patient underwent a medical procedure during which the monitoring device was removed.

Another category of approaches focuses on directly learning from the irregularities by designing specialized model architectures [19–21, 29]. For instance, the GRU-D model incorporates a decaying mechanism within gated recurrent units (GRUs) to better handle irregular sampling intervals [29], while mTAND utilizes multi-time attention to analyze non-uniform measurements effectively [21]. These techniques predominantly capture the correlations within a single sensor’s measurements over time, focusing on intra-series dynamics. Meanwhile, other methods have been proposed to capture inter-series dependencies, modeling explicitly the relationships across sensors within the dataset [19].

Despite these advancements, most approaches tend to specialize in either capturing intra-series dynamics or inter-series relationships, but rarely both simultaneously. Yet, effectively modeling both types of relationships must lead to more accurate predictions and deeper insights. For example, understanding both the individual progression of patients’ vital signs (e.g., heart rate) and how they interact with one another (e.g., the co-dependencies between heart rate and blood pressure over time) can provide a holistic view of a patient’s condition,

*These authors contributed equally.

potentially improving diagnostic accuracy and treatment outcomes. Additionally, in scenarios where one or more sensor observations are missing, irregularity can be compensated by exploiting insights among the correlated sensors.

Inspired by these insights, we introduce **WaveGNN**, a novel framework designed to directly (without imputation) embed irregularly sampled multivariate time series datasets for accurate predictions. WaveGNN captures both the intra-series patterns and the inter-series relationships simultaneously, with two main components. To effectively capture the temporal dependencies of each individual time series, the first component is a Transformer-based encoder. This encoder incorporates a masked attention mechanism that excludes missing data observations during processing, along with a relative timestamp encoding mechanism to capture the time intervals between consecutive observations. Given that more recent observations can be more indicative of the final prediction, a decay mechanism is also incorporated within the encoder to prioritize newer observations. To adequately capture inter-sensor dependencies, the second component of WaveGNN is a dynamic graph neural network, where each node corresponds to a sensor in the dataset, and the edges between nodes denote the correlations between these sensors. These edges are dynamically inferred based on sequence embeddings generated by the transformer-based encoder during the time window and learned global node embeddings shared across all samples and all time windows. Consequently, WaveGNN effectively captures both the dynamic short-term relationships observed within each window and the long-term relationships across the entire dataset, effectively mitigating the impact of missing data by leveraging inter-sensor information.

We evaluate WaveGNN across four real-world healthcare datasets, each associated with distinct classification tasks. Our experiments show that WaveGNN consistently outperforms both imputation-based and specialized state-of-the-art baselines by up to 10.2% in AUPRC and 3.4% in accuracy. Even in real-world scenarios where entire sets of sensor observations are missing, WaveGNN maintains high performance, outperforming baselines with an average relative improvement of 14.7% in F1 score on the challenging PAM dataset, which involves an 8-class classification task. Our ablation study reveals that each proposed component contributes to the overall effectiveness of WaveGNN, with inter-series and intra-series dependencies showing the most significant performance drops when excluded, leading to F1 score reductions of 33.8% and 13.2%, respectively.

2 Related Work

Approaches for handling irregularities in multivariate time series vary widely. Temporal Discretization-based Embedding (TDE) methods transform irregular time series into regular forms through imputation [26]. Such approaches enable the use of standard deep learning models but inherently introduce biases and distort data distributions [24, 27, 28]. To address their shortcomings, approaches such as IP-Net and DGM² proposed using kernel functions to interpolate data against reference points to achieve temporal alignment [25, 30]. Shukla et al. further proposed a time attention mechanism with time embeddings to learn interpolation representations [21], while

Zhang et. al [26] introduced a hybrid model that combines different TDE methods and integrated hand-crafted imputation embeddings into learned interpolation embeddings to improve medical predictions [26]. These approaches still fundamentally rely on imputation, retaining the inherent drawbacks of TDE methods.

Another group of approaches model irregularity directly through specialized algorithms or model architecture designs. To that end, GRU-D employs decaying mechanisms within GRUs to handle the irregular sampling of the data [29]. SeFT applies set function learning to time series classification, treating the series as a set of observations rather than a sequence [20]. Additionally, Raindrop employs graph neural networks to conceptualize multivariate time series as separate sensor graphs, capturing complex inter-variable relationships [19]. While these approaches avoid the TDE drawbacks, they often require extensive customization and typically focus on capturing either intra-variable dynamics or inter-variable dependencies, but not both, potentially overlooking essential data patterns. In contrast, **WaveGNN** introduces a more integrated approach, utilizing a standard transformer architecture with masking and time encoding to effectively model intra-series relationships and a graph neural network architecture to capture short and long-term inter-variable dependencies simultaneously. We evaluate WaveGNN against the aforementioned approaches in Section 5.2.

Graph-based approaches have been extensively applied to model multivariate time series datasets. As an example of dynamic graph-based approaches, BysGNN creates a dynamic multi-context graph for forecasting visits to points of interest (POIs) based on spatial, temporal, semantic, and taxonomic contexts [6]. Similarly, NeuroGNN, captures multi-context correlations in EEG data for seizure classification [4]. These approaches are designed for regular time series data and rely on having external context information to accurately infer inter-series relationships. In contrast, WaveGNN models the inter-series relationships given irregular multivariate time series without requiring additional context.

3 Preliminaries

Definition 1 (Time Series Observation) A time series observation, $s_{i,v}^t$, refers to a single measurement recorded by sensor v at timestamp t for sample i . Sequentially recorded observations over time form a time series $s_{i,v}$ for that sample and sensor.

Definition 2 (Irregular Multivariate Time Series Dataset) Let $D = \{(S_i, t_i, p_i, y_i)\}_{i=1}^N$ be a dataset where each S_i is an irregularly sampled multivariate time series for the i -th sample, $t_i = \{t_{i,v}\}_{v=1}^n$ are the corresponding timestamps, $y_i \in \{1, \dots, C\}$ is the associated categorical outcome label, with C representing the total number of classes, and p_i is an optional set of static features (e.g., patient demographics). Each S_i consists of multiple time series, one for each sensor v . Specifically, $S_i = \{s_{i,v}\}_{v=1}^n$, where $s_{i,v}$ is the time series of observations recorded by sensor v for sample i . The timestamps in $t_{i,v}$ are irregularly spaced, meaning the intervals between consecutive timestamps can vary.

Problem Definition (Irregular Multivariate Time Series

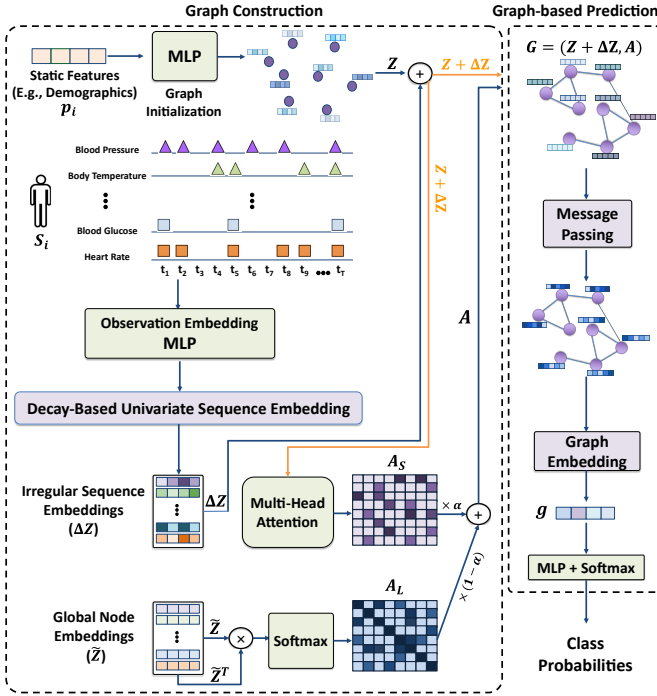


Figure 1: Overall WaveGNN Framework

Prediction Task) Given a dataset $D = \{(S_i, t_i, p_i, y_i)\}_{i=1}^N$ of irregularly sampled multivariate time series, the goal is to learn a function $f: S_i \rightarrow g_i$ that maps the sample s_i , to a fixed-length representation g_i . This representation can be utilized to predict a label $\hat{y}_i \in \{1, \dots, C\}$ relevant to the downstream task.

4 Methodology

Figure 1 presents the end-to-end pipeline of WaveGNN. In the first step, WaveGNN allocates nodes for each sensor, initializing their states using static features from the dataset, like patient demographics, if available, or randomly if not. Next, each sensor’s irregular observation sequence is embedded using a customized Transformer encoder. This encoder employs masked attention, modified temporal encoding, and a decay mechanism to handle irregularities and capture correlations within each sensor’s sequence. The node states are updated based on these sequence embeddings to represent the latent state of each sensor after the observed window. In the third step, WaveGNN establishes edges that represent the correlations across sensors to effectively utilize inter-series correlations. This allows WaveGNN to compensate for missing observations during the input window by leveraging information from other related sensors to each sensor. These edges are formed based on the updated node states, capturing short-term relationships during the observed window, and on learned global node embeddings, capturing long-term relationships derived from the entire training dataset. Next, WaveGNN performs message passing, which updates the node states to incorporate information from these inferred relationships. This process allows each sensor to benefit from

the data captured by other sensors, reducing the impact of irregularity. Finally, the combined node states are aggregated into a single graph-level embedding vector, which is then fed into the prediction head to produce the final prediction. The detailed steps are presented in the following.

4.1 Sensor Graph Construction

Initialization. In WaveGNN, the graph initialization step establishes the preliminary graph structure without connecting any nodes. These will later be updated to reflect the relationships and state of the given sample during the observed time window. The graph comprises nodes, each for a different sensor involved in measuring a time-dependent feature.

For each sample i , each node is initialized with a state vector derived from static features p_i corresponding to the sample (e.g., demographics such as age and gender and clinical contexts such as ICU types in the medical downstream tasks). If this information is not available for a task, the vectors are initialized randomly. These features are transformed using a two-layer MLP with ReLU activations to create high-dimensional representations that encapsulate the sample’s baseline characteristics and provide a sample-specific initial context for the task:

$$Z_i = \text{MLP}(p_i) \quad (1)$$

Here, p_i represents the sample i ’s static features and $Z_i = \{z_{i,1}, \dots, z_{i,n}\} \in \mathbb{R}^{n \times M}$ represents the matrix of initial state vectors for all nodes where M is the embedding dimension.

Observation Embedding. For sample i , for each sensor v , let the observation at time t be denoted as $s_{i,v}^t$. To enhance the expressive power of our model [31], each observation is mapped to a higher-dimensional space using an MLP with tanh activations:

$$h_{i,v}^t = \text{MLP}(s_{i,v}^t) \quad (2)$$

We use tanh activation to ensure that embeddings are centered around zero, which helps in capturing the inconsistencies in the observations. For instance, two observations that are inconsistent with each other can result in embeddings that are oppositely signed.

Temporal Encoding. To effectively capture the temporal dynamics and patterns within each sensor’s time series, we augment the observation embeddings with time information. Inspired by GRU-D [29], we similarly embed the relative timestamps that reflect the time difference between consecutive observations for each sensor.

To represent these time differences, we apply Time2Vec [32], which encodes the time information into a vector. Time2Vec includes two components: a sinusoidal component that captures periodic patterns, and a non-periodic transformation component that captures non-periodic patterns and time gaps. This dual encoding enables the model to incorporate both regular temporal cycles and irregular time gaps between observations. This turns the time intervals themselves into a valuable source of information rather than merely considering the relative position of observations, as done in the original Transformer [33].

For each observation at time $t_{v,j}$, where v indicates the sensor and j the index of the observation, we compute the time delta $\delta t_{v,j} = t_{v,j} - t_{v,j-1}$ as the difference between the current observation time and the previous observation time for that sensor. The time encoding vector $e_{\delta t_{v,j}}$ is then computed as:

$$e_{\delta t_{v,j}} = \text{Time2Vec}(\delta t_{v,j}) \quad (3)$$

Augmenting observation embeddings with $e_{\delta t_{v,j}}$ equips the model to better recognize and utilize the underlying temporal structure in the data.

Decay-Based Univariate Sequence Embedding. In order to capture the intra-series correlations, we embed each irregular sequence of observations from each sensor separately. Given the sequence of T observation embeddings $(h_{i,v}^{t_1}, \dots, h_{i,v}^{t_T}) \in \mathbb{R}^{T \times M}$ for sample i and sensor v , we add the temporal encoding information to the observation embeddings. For simplicity, we omit the sample index i in the following equations:

$$h_v^{t_j} \leftarrow h_v^{t_j} + e_{\delta t_{v,j}} \quad \forall j \in \{1, 2, \dots, T\} \quad (4)$$

Next, we pass the time-augmented sequence $H_v = (h_v^{t_1}, \dots, h_v^{t_T}) \in \mathbb{R}^{T \times M}$ through a Transformer encoder, using the mask vector $M_v = (m_{v,1}, \dots, m_{v,T}) \in \mathbb{R}^T$ as a padding mask. Here, each $m_{v,j}$ indicates whether there was an observation at time t_j for sensor v (1 if present, 0 if missing). If the observation is missing, the corresponding $h_v^{t_j}$ is a zero-filled place-holder vector. This way, the Transformer’s attention mechanism focuses only on the actual observations, effectively ignoring the missing ones while embedding the real observations:

$$Z_v = \text{TransformerEncoder}(H_v, M_v) \quad (5)$$

The output sequence $Z_v = (z_v^{t_1}, \dots, z_v^{t_T})$ captures the intra-series correlations, with the attention mechanism ensuring that the presence of missing observations does not negatively affect the representation of the observed data.

Following this, WaveGNN utilizes a decay-based weighting scheme to aggregate the new sequence of embeddings into a single vector. This ensures that more recent observations have a greater influence on the final representation, as they provide the most up-to-date information about the sample. Moreover, WaveGNN’s weighting accounts for the irregular time intervals between observations, considering that observations with shorter intervals between them should have similar impacts on the final embedding, whereas those with larger time gaps should be weighted differently.

To this end, WaveGNN first calculates the time differences of each observation from the most recent observation $t_{v,T}$:

$$\delta t'_{v,j} = t_{v,T} - t_{v,j} \quad (6)$$

Next, we compute an observation weight at $t_{v,j}$ as follows:

$$w_{v,j} = m_{v,j} \cdot e^{-\eta \times \delta t'_{v,j}} \quad (7)$$

where η is a learned parameter that controls the decay rate. Mask value $m_{v,j}$ is multiplied so the missing observations are ignored. The exponential function is used because it provides a smooth decay of weights controlled by η as the time

differences increase, ensuring that observations further away from the most recent time have smaller weights.

Finally, we normalize the weights using a softmax function so that they sum up to 1:

$$\tilde{w}_{v,j} = \frac{m_{v,j} \cdot e^{-\eta \times \delta t'_{v,j}}}{\sum_{k=1}^T m_{v,k} \cdot e^{-\eta \times \delta t'_{v,k}}} \quad (8)$$

We then aggregate the embeddings to obtain a single vector representation for the sequence using the calculated weights:

$$\Delta z_v = \sum_{j=1}^T \tilde{w}_{v,j} \cdot z_v^{t_j} \quad (9)$$

The final embedding vector Δz_v effectively captures the intra-series dependencies and the importance of each observation in sensor v . This representation is then used to update the node state vector for the sensor:

$$z_{i,v} \leftarrow z_{i,v} + \Delta z_v \quad (10)$$

This update is applied in a residual manner to enhance the gradient flow during training and allow the model to refine the initial context derived from static features with information from the actual observations.

Inferring Inter-series Relationships. Now that node states are updated, WaveGNN infers the inter-node relationships by combining two distinct types of adjacency matrices, each representing the relationships from a different perspective:

- **Dynamic Short-Term Dependencies (A_S):** This matrix is derived from the multi-head attention mechanism [33] applied to the updated node states. It captures the temporal similarity across node states of different sensors within the observed window, reflecting immediate, short-term dependencies among the nodes. This approach has been shown to be effective in capturing dynamic node relationships [4,6,34].

$$A_S = \text{Multihead_Attention}(\text{keys} = Z, \text{queries} = Z) \quad (11)$$

- **Static Long-Term Similarities (A_L):** WaveGNN learns global node embeddings $\tilde{Z} = \{\tilde{z}_1, \dots, \tilde{z}_n\} \in \mathbb{R}^{n \times M}$, where M is the embedding dimension. These embeddings reflect long-term similarities between sensors, learned from the entire dataset for a specific downstream task. The A_L matrix is then computed using the dot product between these global node embeddings, followed by a softmax normalization:

$$A_L = \text{softmax}(\tilde{Z} \times \tilde{Z}^T) \quad (12)$$

The final adjacency matrix A is formed by combining the two similarity matrices using a learnable parameter α :

$$A = \alpha A_S + (1 - \alpha) A_L \quad (13)$$

This allows the model to learn which of these similarities are more important in the downstream task. Finally, we zero out the smallest $K\%$ of the elements in A to make the resulting adjacency matrix sparser.

4.2 Graph-based Prediction

With the updated node states Z and adjacency matrix A , the graph $G = (Z, A)$ for the given window of observations is constructed, encapsulating the latest node states and their inter-relationships. We perform GNN-based message passing on this graph to capture the node relationships within the node embeddings. Afterward, we apply pooling and transformations to obtain a single embedding vector representing all important node embeddings. The final embedding is used to make the prediction.

Message Passing. To perform message passing, the graph is passed through a GNN block that utilizes a modified Graph Convolutional Networks (GCN) variant [35]. In this variant, we remove the normalization term and add residual connections between the message-passing layers to preserve directed relationships in the graph and mitigate oversmoothing [36], respectively. This yields the node embeddings matrix $V \in \mathbb{R}^{n \times M'}$, where M' represents the embedding dimension.

Graph Embedding. To derive a graph-level representation from the node embeddings, two operations are performed:

- **Max Pooling:** Applied to the node embeddings to extract the most significant features, helping to capture the most expressive node attributes relevant to the prediction task.
- **Transformation:** All node embeddings are concatenated into a single vector, which is then transformed via an MLP to integrate information across all nodes.

Final Prediction. The final l -dimensional graph-level representation $g \in \mathbb{R}^l$ is obtained by first concatenating the outputs of the max pooling layer and the MLP-transformed concatenated embeddings, followed by an MLP layer for dimensionality reduction.

Finally, the graph-level embedding g is utilized for the downstream task of interest. In our approach, we pass this through another MLP to predict the label of the samples:

$$\hat{y} = MLP(g) \quad (14)$$

Where \hat{y} represents the predicted class probabilities.

5 Experiments

5.1 Experimental Setup

Datasets and Evaluation Setup. We evaluate WaveGNN on four real-world healthcare datasets. **P12** [37] and **MIMIC III** [38] contain ICU patient data, with labels indicating survival during hospitalization (48-IHM). MIMIC III also includes labels for multilabel phenotype classification (24-PHE). **P19** [39] focuses on sepsis detection, while **PAM** [40] is an activity monitoring dataset with labels for different activities. P12, P19, and MIMIC III are naturally irregular datasets, while irregularity in PAM is introduced artificially. The dataset statistics are presented in Table 1. For a fair comparison, we followed the same preprocessing steps with previous studies [19, 28], and adopted the same dataset splits. To that extent, the training, validation, and testing ratios for P12, P19, and PAM is 80:10:10, and 85:7.5:7.5 for MIMIC III. The indices of these splits are fixed across all methods and experiments. Evaluation metrics also match those used in

prior studies to maintain consistency, and all hyperparameters were kept the same across all datasets and experiments. More details regarding the evaluation setup and hyperparameter tuning can be found in the Supplementary Material sections A.1-A.3.

Table 1: Statistics of the datasets used in experimental study.

Statistics	MIMIC III	P12	P19	PAM
# of samples	16,143	11,988	38,803	5,333
# of timestamps	≤ 700	215	60	600
# of sensors	17	36	34	17
static info	False	True	True	False
missing ratio (%)	72.07	88.40	94.90	60.00
imbalanced	True	True	True	False
# of classes	2 (IHM) / 25 (PHE)	2	2	8

Baselines. We compare WaveGNN to 8 methods: *IP-Net* [41], *DGM²-O* [30], *mTAND* [42] and *UTDE* [26] are imputation-based baselines, while *GRU-D* [29], *SeFT* [20], *MTGNN* [43], and *Raindrop* [19], are specialized models designed to handle irregularly sampled datasets. UTDE and Raindrop are considered the state-of-the-art imputation-based and specialized model approaches, respectively.

5.2 Results

Overall Performance. We report the overall performance of WaveGNN and baselines in Tables 2 and 3, where the **best** and **second best** values are highlighted. WaveGNN consistently outperforms the baselines in the majority of cases (9 out of 12 experiments), and when it doesn't, its performance is very close to the best-performing baseline.

Notably, WaveGNN achieves significant improvements in AUPRC, with gains of 10.2% and 2.4% over the best baseline in the binary tasks on the P19 and P12 datasets, respectively. In the multi-class task on the PAM dataset, WaveGNN consistently outperforms all baselines, demonstrating performance improvements of over 3.3% across all metrics. The PAM dataset has the smallest missing ratio and very long sequences among the evaluated datasets. This highlights that WaveGNN is highly effective not only in challenging scenarios like P19, which has over a 94% missing ratio and short sequences, but also in cases with less irregularity.

The results on the binary 48-IHM task of the MIMIC dataset are mixed. While WaveGNN outperforms UTDE by 2.64% in terms of F1 score, UTDE performs better in terms of AUPRC. This can be attributed to MIMIC's longer sequences of observations with a lower missing data ratio compared to the P12 and P19 binary tasks, making imputation-based methods more effective for this less challenging binary classification task. However, in the more challenging multi-label classification task of 24-PHE on the same dataset, WaveGNN outperforms UTDE by a margin of 23.7% in F1 score, demonstrating that imputation-based methods become less effective in more complex scenarios.

In sum, on datasets with lower missing data ratios and longer sequences, like MIMIC and PAM, imputation-based methods like UTDE tend to outperform specialized models. Conversely, on datasets with higher missing data ratios, such

Table 2: Performance comparison with the state-of-the-art on P12, P19, and PAM datasets. P12 and P19 are evaluated on mortality and sepsis prediction, respectively, based on the AUROC and AUPRC metrics. The PAM dataset is evaluated on activity classification in terms of (weighted) Accuracy, Precision, Recall, and F1 Score. The reported values are averaged across 3 independent runs. **Best** and second best values are highlighted.

Methods	P12		P19		PAM			
	AUROC	AUPRC	AUROC	AUPRC	Accuracy	Precision	Recall	F1 score
GRU-D	81.9 ± 3.6	46.1 ± 4.7	83.9 ± 1.7	46.9 ± 2.1	83.3 ± 1.6	84.6 ± 1.2	85.2 ± 1.6	84.8 ± 1.2
SeFT	73.9 ± 2.5	31.1 ± 4.1	78.7 ± 2.4	31.1 ± 2.8	67.1 ± 2.2	70.0 ± 2.4	68.2 ± 1.5	68.5 ± 1.8
mTAND	84.2 ± 0.8	48.2 ± 3.4	80.4 ± 1.3	32.4 ± 1.8	74.6 ± 4.3	74.3 ± 4.0	79.5 ± 2.8	76.8 ± 3.4
IP-Net	82.6 ± 1.4	47.6 ± 3.1	84.6 ± 1.3	38.1 ± 3.7	74.3 ± 3.8	75.6 ± 2.1	77.9 ± 2.2	76.6 ± 2.8
DGM ² -O	84.4 ± 1.6	47.3 ± 3.1	86.7 ± 3.4	44.7 ± 11.7	82.4 ± 2.3	85.2 ± 1.2	83.9 ± 2.3	84.3 ± 1.8
MTGNN	74.4 ± 6.7	35.5 ± 6.0	81.9 ± 6.2	39.9 ± 8.9	83.4 ± 1.9	85.2 ± 1.7	86.1 ± 1.9	85.9 ± 2.4
Raindrop	82.8 ± 1.7	44.0 ± 3.0	87.0 ± 2.3	<u>51.8 ± 5.5</u>	88.5 ± 1.5	89.9 ± 1.5	89.9 ± 0.6	89.8 ± 1.0
UTDE	81.1 ± 2.2	45.9 ± 2.1	84.3 ± 3.1	41.1 ± 6.0	90.4 ± 1.8	90.7 ± 1.8	90.4 ± 1.8	90.4 ± 1.8
WaveGNN	83.9 ± 1.2	49.4 ± 1.5	88.0 ± 0.9	57.1 ± 4.7	93.5 ± 1.1	93.7 ± 1.1	93.5 ± 1.1	93.5 ± 1.1
<i>Improvement</i>	-0.59%	+2.48%	+1.14%	+10.23%	+3.42%	+3.30%	+3.42%	+3.42%

Table 3: Performance comparison with the state-of-the-art on MIMIC III dataset, for 48-IHM and 24-PHE tasks. The performance of 48-IHM is measured on F1 and AUPRC, and 24-PHE on F1 (Macro) and AUROC. We report the average results across 3 independent runs. **Best** and second best values are highlighted.

Methods	48-IHM		24-PHE	
	F1	AUPRC	F1	AUROC
GRU-D	42.8 ± 0.6	45.9 ± 0.4	19.0 ± 1.0	73.3 ± 0.1
SeFT	16.5 ± 8.6	23.9 ± 0.5	6.1 ± 0.2	65.7 ± 0.1
mTAND	43.9 ± 0.5	47.5 ± 1.3	19.9 ± 0.4	73.5 ± 0.1
IP-Net	37.2 ± 2.8	39.4 ± 1.1	17.9 ± 0.7	73.5 ± 0.1
DGM ² -O	39.1 ± 1.5	37.8 ± 1.5	18.4 ± 0.2	71.7 ± 0.2
MTGNN	38.6 ± 2.5	36.5 ± 2.1	14.5 ± 1.7	70.6 ± 0.7
Raindrop	39.5 ± 3.7	36.2 ± 0.4	21.8 ± 1.7	74.0 ± 0.9
UTDE	45.3 ± 0.7	49.6 ± 1.0	24.9 ± 0.4	75.6 ± 0.2
WaveGNN	46.5 ± 0.9	47.8 ± 1.3	30.8 ± 0.2	74.9 ± 0.1
<i>Improvement</i>	+2.64%	-3.62%	+23.69%	-0.93%

as P19, specialized models like Raindrop are more effective. This makes sense: with more observations, imputation can more accurately estimate missing values, whereas in cases with fewer observations, the biased assumptions of imputation methods become less effective, making direct modeling approaches more suitable. Notably, WaveGNN consistently outperforms the best of both methods across all datasets.

Leave-sensors-out settings. We also evaluate WaveGNN under more challenging scenarios where whole sensor observations are missing. This simulates real-world cases where some sensors fail or are unavailable. Following the approach adopted by Raindrop [19], we experimented with two setups on PAM dataset. In the first one, we remove all the observations for a fixed set of the most informative sensors from samples, while in the second setting, we remove all the observations for a random set of sensors. Table 4 presents the results for both cases when 10%, 30%, and 50% of the sen-

sors are removed. Our approach outperforms the baselines in 23 out of 24 experiments and ranks second in only one case. Specifically, WaveGNN demonstrates notable improvements, with up to 15.5% relative improvement in F1 score compared to the best baseline with 10% missing sensors, and up to 45.2% and 7.5% improvement for cases with 30% and 50% missing sensors, respectively.

Among the baselines, Raindrop remains the strongest competitor to WaveGNN. This shows the importance of capturing inter-series relationships and highlights the effectiveness of graph-based modeling. By successfully capturing the dependencies between sensors, missing data can be compensated, leveraging insights from correlated sensors that are relevant to the final outcome. In contrast, imputation-based methods, like mTAND and UTDE, demonstrate the largest performance degradation as the missing sensor ratio increases. These approaches still try to fill in the missing values, but with entire sensor observations missing, they have little to no reliable data to base their imputations on. This leads to inaccurate or biased reconstructions and, hence, affects their performance.

5.3 Ablation Study

We created different variations of WaveGNN to understand the effectiveness of its different components: *w/o short-term* and *w/o long-term* variants remove the A_S and A_L similarity matrices, so that the short- and long-term inter-series relationships are not considered, respectively. The *w/o inter-series* variant excludes the graph message passing part, so neither of the inter-series similarity measures are considered, while the *w/o intra-series* variant removes the transformer-based module and simply aggregates the observation embeddings for each sensor to obtain a univariate sequence embedding. Finally, the *w/o temporal encoding* variant discards the temporal encoding module and uses a simple positional encoding for the Transformer, and the *w/o decay rate* variant removes WaveGNN’s decay mechanism, aggregating the output sequence embedding of the Transformer with equal weights, thus treating all observations in a sequence equally.

Table 4: Performance comparison on the PAM dataset under different missing sensor ratios and different settings. We report the average results across 3 independent runs. **Best** and second best values are highlighted.

Experiment Setting		Leave-fixed-sensors-out				Leave-random-sensors-out			
Missing sensor ratio	Methods	Accuracy	Precision	Recall	F1 score	Accuracy	Precision	Recall	F1 score
10%	GRU-D	65.4 ± 1.7	72.6 ± 2.6	64.3 ± 5.3	63.6 ± 0.4	68.4 ± 3.7	74.2 ± 3.0	70.8 ± 4.2	72.0 ± 3.7
	SeFT	58.9 ± 2.3	62.5 ± 1.8	59.6 ± 2.6	59.6 ± 2.6	40.0 ± 1.9	40.8 ± 3.2	41.0 ± 0.7	39.9 ± 1.5
	mTAND	58.8 ± 2.7	59.5 ± 5.3	64.4 ± 2.9	61.8 ± 4.1	53.4 ± 2.0	54.8 ± 2.7	57.0 ± 1.9	55.9 ± 2.2
	RAINDROP	77.2 ± 2.1	82.3 ± 1.1	78.4 ± 1.9	75.2 ± 3.1	76.7 ± 1.8	79.9 ± 1.7	77.9 ± 2.3	78.6 ± 1.8
	UTDE	71.8 ± 1.7	76.5 ± 2.6	71.8 ± 1.7	70.6 ± 2.3	74.5 ± 1.9	75.9 ± 2.1	74.5 ± 1.9	74.6 ± 2.1
	WaveGNN	86.9 ± 2.2	88.0 ± 1.3	86.9 ± 2.2	86.9 ± 3.3	82.2 ± 1.5	83.9 ± 0.8	82.2 ± 1.5	82.5 ± 1.3
	<i>Improvement</i>		+12.56%	+6.92%	+10.84%	+15.55%	+7.17%	+5.00%	+5.51%
30%	GRU-D	45.1 ± 2.9	51.7 ± 6.2	42.1 ± 6.6	47.2 ± 3.9	58.0 ± 2.0	63.2 ± 1.7	58.2 ± 3.1	59.3 ± 3.5
	SeFT	32.7 ± 2.3	27.9 ± 2.4	34.5 ± 3.0	28.0 ± 1.4	31.7 ± 1.5	31.0 ± 2.7	32.0 ± 1.2	28.0 ± 1.6
	mTAND	27.5 ± 4.5	31.2 ± 7.3	30.6 ± 4.0	30.8 ± 5.6	34.7 ± 5.5	43.4 ± 4.0	36.3 ± 4.7	39.5 ± 4.4
	RAINDROP	52.4 ± 2.8	60.9 ± 3.8	51.3 ± 1.6	48.4 ± 5.6	60.3 ± 3.3	68.1 ± 4.6	60.3 ± 3.3	60.3 ± 3.3
	UTDE	41.2 ± 2.9	46.9 ± 6.5	41.2 ± 2.9	35.7 ± 3.9	57.9 ± 2.5	65.0 ± 3.4	57.9 ± 2.5	58.4 ± 2.8
	WaveGNN	71.2 ± 2.8	75.7 ± 3.4	71.2 ± 2.8	70.3 ± 3.2	68.6 ± 1.6	75.1 ± 1.8	68.6 ± 1.6	69.0 ± 1.3
	<i>Improvement</i>		+35.87%	+24.30%	+38.79%	+45.24%	+13.76%	+10.27%	+13.76%
50%	GRU-D	37.3 ± 2.7	29.6 ± 5.9	32.8 ± 4.6	26.6 ± 5.9	49.7 ± 1.2	52.4 ± 0.3	42.5 ± 1.7	47.5 ± 1.2
	SeFT	24.7 ± 1.1	15.9 ± 2.7	25.3 ± 2.6	18.2 ± 2.4	26.4 ± 1.4	23.0 ± 2.9	27.5 ± 0.4	23.5 ± 1.8
	mTAND	16.9 ± 3.1	12.6 ± 5.5	17.0 ± 1.6	13.9 ± 4.0	20.9 ± 3.1	35.1 ± 6.1	23.0 ± 3.2	27.7 ± 3.9
	RAINDROP	46.6 ± 2.6	44.5 ± 2.6	42.4 ± 3.9	38.0 ± 4.0	47.2 ± 4.4	59.4 ± 3.9	44.8 ± 3.5	47.6 ± 5.2
	UTDE	30.6 ± 2.4	32.9 ± 13.5	30.6 ± 2.4	25.1 ± 3.9	43.5 ± 1.7	52.7 ± 4.0	43.5 ± 1.7	43.2 ± 1.9
	WaveGNN	43.2 ± 3.5	46.6 ± 6.1	43.2 ± 3.5	38.2 ± 3.4	51.2 ± 3.3	63.3 ± 5.1	51.2 ± 3.3	51.2 ± 3.3
	<i>Improvement</i>		-7.29%	+4.71%	+1.88%	+0.52%	+3.01%	+6.56%	+14.28%

Table 5 presents the results of the ablation study on the PAM dataset, showing the impact of removing various components of WaveGNN. Our findings indicate that all components contribute to improved performance, with the most significant drops occurring when inter-series and intra-series relationships are removed, leading to performance decreases of 33.8% and 13.2% in weighted F1 score, respectively. This shows the importance of simultaneously addressing both intra-variable dynamics and inter-variable dependencies to effectively model irregular datasets.

Interestingly, the removal of dynamic short-term dependencies has a greater negative impact on performance than the removal of long-term dependencies. This outcome is intuitive, as short-term dependencies between sensors within the current input window are often more critical than long-term dependencies, given their specificity to the individual sample and time window, rather than being generalized across all samples and time periods. For example, the relationship between a patient’s heart rate and blood sugar level during a particular time window might differ from the typical pattern usually seen in that patient, possibly due to the effects of medication or other factors, making it more relevant to focus on these short-term dependencies.

Lastly, both the temporal encoding and the decay mechanism components are integral to WaveGNN’s overall performance. Temporal encoding allows the model to capture the temporal dynamics and patterns within each sensor’s time series, while the decay mechanism ensures that more recent data, which is often more indicative of final outcomes, is given appropriate weight. Together, these components enable WaveGNN to manage the timing and relevance of observations effectively, contributing to overall performance.

Table 5: Ablation study results on the PAM dataset. We report the average results across 3 independent runs.

Ablation Setting	Accuracy	Precision	Recall	F1 score
w/o short-term	89.9 ± 1.9	90.1 ± 1.9	89.9 ± 1.9	89.8 ± 2.0
w/o long-term	92.3 ± 1.9	92.4 ± 1.9	92.3 ± 1.9	92.2 ± 1.9
w/o inter-series	64.1 ± 1.7	63.5 ± 2.0	64.1 ± 3.1	61.9 ± 3.1
w/o intra-series	81.2 ± 1.3	81.5 ± 1.5	81.2 ± 1.3	81.2 ± 1.4
w/o temporal encoding	90.6 ± 1.1	90.6 ± 1.0	90.6 ± 1.1	90.4 ± 1.2
w/o decay rate	90.6 ± 2.3	90.7 ± 2.3	90.6 ± 2.3	90.5 ± 2.3
WaveGNN	93.5 ± 1.1	93.7 ± 1.1	93.5 ± 1.1	93.5 ± 1.1

6 Conclusion

In this study, we introduced WaveGNN, a novel framework designed to directly embed irregularly sampled multivariate time series datasets for accurate predictions. Unlike previous imputation-based and specialized model approaches, WaveGNN simultaneously captures both intra-series correlations and inter-series relationships, enabling the model to effectively compensate for missing observations. Our evaluation demonstrated that WaveGNN outperforms state-of-the-art baselines across diverse datasets, even under conditions of extreme sparsity where entire sensors are missing, thereby validating the importance of each proposed component within the framework. In the future, we plan to expand WaveGNN to support multimodal scenarios.

References

- [1] Shadab Alam, Franco D Albareti, Carlos Allende Prieto, Friedrich Anders, Scott F Anderson, Timothy Anderton, Brett H Andrews, Eric Armengaud, Éric Aubourg, Stephen Bailey, et al. The eleventh and twelfth data

- releases of the sloan digital sky survey: final data from sdss-iii. *The Astrophysical Journal Supplement Series*, 219(1):12, 2015.
- [2] Bharat B Biswal, Maarten Mennes, Xi-Nian Zuo, Suril Gohel, Clare Kelly, Steve M Smith, Christian F Beckmann, Jonathan S Adelstein, Randy L Buckner, Stan Colcombe, et al. Toward discovery science of human brain function. *Proceedings of the national academy of sciences*, 107(10):4734–4739, 2010.
 - [3] Parsa Razmara, Tina Khezresmaeilzadeh, and B Keith Jenkins. Fever detection with infrared thermography: Enhancing accuracy through machine learning techniques. In *IEEE-EMBS International Conference on Biomedical and Health Informatics*.
 - [4] Arash Hajisafi, Haowen Lin, Yao-Yi Chiang, and Cyrus Shahabi. Dynamic gns for precise seizure detection and classification from eeg data. In *Pacific-Asia Conference on Knowledge Discovery and Data Mining*, pages 207–220. Springer, 2024.
 - [5] Arash Hajisafi, Maria Despoina Siampou, Jize Bi, Luciano Nocera, and Cyrus Shahabi. Wearables for health (w4h) toolkit for acquisition, storage, analysis and visualization of data from various wearable devices. In *ICDE*, 2024.
 - [6] Arash Hajisafi, Haowen Lin, Sina Shaham, Haoji Hu, Maria Despoina Siampou, Yao-Yi Chiang, and Cyrus Shahabi. Learning dynamic graphs from all contextual information for accurate point-of-interest visit forecasting. In *Proceedings of the 31st ACM International Conference on Advances in Geographic Information Systems*, pages 1–12, 2023.
 - [7] Maria Despoina Siampou, Chrysovalantis Anastasiou, John Krumm, and Cyrus Shahabi. Trajroute: Rethinking routing with a simple trajectory-based approach—forget the maps and traffic! *arXiv preprint arXiv:2411.01325*, 2024.
 - [8] Maria Despoina Siampou, Luciano Nocera, Jinseok Oh, Beth Smith A., and Cyrus Shahabi. An algorithmic approach for detecting neuromotor developmental disabilities in infants from wearable sensor data. In *International Conference of the IEEE Engineering in Medicine and Biology Society (EMBC)*, 2024.
 - [9] Yaguang Li, Rose Yu, Cyrus Shahabi, and Yan Liu. Diffusion convolutional recurrent neural network: Data-driven traffic forecasting. *arXiv preprint arXiv:1707.01926*, 2017.
 - [10] Rosario N Mantegna. Hierarchical structure in financial markets. *The European Physical Journal B-Condensed Matter and Complex Systems*, 11:193–197, 1999.
 - [11] Omer Berat Sezer, Mehmet Ugur Gudelek, and Ahmet Murat Ozbayoglu. Financial time series forecasting with deep learning: A systematic literature review: 2005–2019. *Applied soft computing*, 90:106181, 2020.
 - [12] Eduardo J Ruiz, Vagelis Hristidis, Carlos Castillo, Aristides Gionis, and Alejandro Jaimes. Correlating financial time series with micro-blogging activity. In *Proceedings of the fifth ACM international conference on Web search and data mining*, pages 513–522, 2012.
 - [13] Dennis Shasha. Tuning time series queries in finance: Case studies and recommendations. *IEEE Data Eng. Bull.*, 22(2):40–46, 1999.
 - [14] Pablo Huijse, Pablo A Estevez, Pavlos Protopapas, Jose C Principe, and Pablo Zegers. Computational intelligence challenges and applications on large-scale astronomical time series databases. *IEEE Computational Intelligence Magazine*, 9(3):27–39, 2014.
 - [15] Gabriel Wachman, Roni Khardon, Pavlos Protopapas, and Charles R Alcock. Kernels for periodic time series arising in astronomy. In *Machine Learning and Knowledge Discovery in Databases: European Conference, ECML PKDD 2009, Bled, Slovenia, September 7-11, 2009, Proceedings, Part II 20*, pages 489–505. Springer, 2009.
 - [16] Haoyi Zhou, Shanghang Zhang, Jieqi Peng, Shuai Zhang, Jianxin Li, Hui Xiong, and Wancai Zhang. Informer: Beyond efficient transformer for long sequence time-series forecasting. In *Proceedings of the AAAI conference on artificial intelligence*, volume 35, pages 11106–11115, 2021.
 - [17] Bing Yu, Haoteng Yin, and Zhanxing Zhu. Spatio-temporal graph convolutional networks: A deep learning framework for traffic forecasting. *arXiv preprint arXiv:1709.04875*, 2017.
 - [18] Ling Zhao, Yujiao Song, Chao Zhang, Yu Liu, Pu Wang, Tao Lin, Min Deng, and Haifeng Li. T-gcn: A temporal graph convolutional network for traffic prediction. *IEEE transactions on intelligent transportation systems*, 21(9):3848–3858, 2019.
 - [19] Xiang Zhang, Marko Zeman, Theodoros Tsiligkaridis, and Marinka Zitnik. Graph-guided network for irregularly sampled multivariate time series. In *International Conference on Learning Representations*, 2021.
 - [20] Max Horn, Michael Moor, Christian Bock, Bastian Rieck, and Karsten Borgwardt. Set functions for time series. In *International Conference on Machine Learning*, pages 4353–4363. PMLR, 2020.
 - [21] Satya Narayan Shukla and Benjamin Marlin. Multi-time attention networks for irregularly sampled time series. In *International Conference on Learning Representations*, 2020.
 - [22] Wenjie Hu, Yang Yang, Ziqiang Cheng, Carl Yang, and Xiang Ren. Time-series event prediction with evolutionary state graph. In *Proceedings of the 14th ACM International Conference on Web Search and Data Mining*, pages 580–588, 2021.
 - [23] Zekun Li, Shiyang Li, and Xifeng Yan. Time series as images: Vision transformer for irregularly sampled time series. *Advances in Neural Information Processing Systems*, 36, 2024.
 - [24] Zachary C Lipton, David Kale, and Randall Wetzel. Directly modeling missing data in sequences with rnns:

- Improved classification of clinical time series. In *Machine learning for healthcare conference*, pages 253–270. PMLR, 2016.
- [25] Satya Narayan Shukla and Benjamin M Marlin. Interpolation-prediction networks for irregularly sampled time series. *arXiv preprint arXiv:1909.07782*, 2019.
- [26] Xinlu Zhang, Shiyang Li, Zhiyu Chen, Xifeng Yan, and Linda Ruth Petzold. Improving medical predictions by irregular multimodal electronic health records modeling. In *International Conference on Machine Learning*, pages 41300–41313. PMLR, 2023.
- [27] Matthew McDermott, Bret Nestor, Evan Kim, Wancong Zhang, Anna Goldenberg, Peter Szolovits, and Marzyeh Ghassemi. A comprehensive ehr timeseries pre-training benchmark. In *Proceedings of the Conference on Health, Inference, and Learning*, pages 257–278, 2021.
- [28] Hrayr Harutyunyan, Hrant Khachatrian, David C Kale, Greg Ver Steeg, and Aram Galstyan. Multitask learning and benchmarking with clinical time series data. *Scientific data*, 6(1):96, 2019.
- [29] Zhengping Che, Sanjay Purushotham, Kyunghyun Cho, David Sontag, and Yan Liu. Recurrent neural networks for multivariate time series with missing values. *Scientific reports*, 8(1):6085, 2018.
- [30] Yinjun Wu, Jingchao Ni, Wei Cheng, Bo Zong, Dongjin Song, Zhengzhang Chen, Yanchi Liu, Xuchao Zhang, Haifeng Chen, and Susan B Davidson. Dynamic gaussian mixture based deep generative model for robust forecasting on sparse multivariate time series. In *Proceedings of the AAAI Conference on Artificial Intelligence*, volume 35, pages 651–659, 2021.
- [31] Petar Veličković, Guillem Cucurull, Arantxa Casanova, Adriana Romero, Pietro Liò, and Yoshua Bengio. Graph attention networks. In *International Conference on Learning Representations*, 2018.
- [32] Seyed Mehran Kazemi, Rishab Goel, Sepehr Eghbali, Janahan Ramanan, Jaspreet Sahota, Sanjay Thakur, Stella Wu, Cathal Smyth, Pascal Poupert, and Marcus Brubaker. Time2vec: Learning a vector representation of time. *arXiv preprint arXiv:1907.05321*, 2019.
- [33] Ashish Vaswani, Noam Shazeer, Niki Parmar, Jakob Uszkoreit, Llion Jones, Aidan N Gomez, Łukasz Kaiser, and Illia Polosukhin. Attention is all you need. *Advances in neural information processing systems*, 30, 2017.
- [34] Petar Veličković, Guillem Cucurull, Arantxa Casanova, Adriana Romero, Pietro Lio, and Yoshua Bengio. Graph attention networks. *arXiv preprint arXiv:1710.10903*, 2017.
- [35] T. N. Kipf and M. Welling. Semi-supervised classification with graph convolutional networks. In *ICLR*, 2017.
- [36] D. Chen and et al. Measuring and relieving the over-smoothing problem for graph neural networks from the topological view. In *AAAI*, volume 34, pages 3438–3445, 2020.
- [37] Ary L Goldberger, Luis AN Amaral, Leon Glass, Jeffrey M Hausdorff, Plamen Ch Ivanov, Roger G Mark, Joseph E Mietus, George B Moody, Chung-Kang Peng, and H Eugene Stanley. Physiobank, physiotookit, and physionet: components of a new research resource for complex physiologic signals. *circulation*, 101(23):e215–e220, 2000.
- [38] Alistair EW Johnson, Tom J Pollard, Lu Shen, Li-wei H Lehman, Mengling Feng, Mohammad Ghassemi, Benjamin Moody, Peter Szolovits, Leo Anthony Celi, and Roger G Mark. Mimic-iii, a freely accessible critical care database. *Scientific data*, 3(1):1–9, 2016.
- [39] Matthew A Reyna, Christopher S Josef, Russell Jeter, Supreeth P Shashikumar, M Brandon Westover, Shamim Nemati, Gari D Clifford, and Ashish Sharma. Early prediction of sepsis from clinical data: the physionet/computing in cardiology challenge 2019. *Critical care medicine*, 48(2):210–217, 2020.
- [40] Attila Reiss and Didier Stricker. Introducing a new benchmarked dataset for activity monitoring. In *2012 16th international symposium on wearable computers*, pages 108–109. IEEE, 2012.
- [41] Satya Narayan Shukla and Benjamin M Marlin. Interpolation-prediction networks for irregularly sampled time series. *arXiv preprint arXiv:1909.07782*, 2019.
- [42] Satya Narayan Shukla and Benjamin M Marlin. Multi-time attention networks for irregularly sampled time series. *arXiv preprint arXiv:2101.10318*, 2021.
- [43] Zonghan Wu, Shirui Pan, Guodong Long, Jing Jiang, Xiaojun Chang, and Chengqi Zhang. Connecting the dots: Multivariate time series forecasting with graph neural networks. In *Proceedings of the 26th ACM SIGKDD international conference on knowledge discovery & data mining*, pages 753–763, 2020.